

The Accuracy of Near Infrared Spectroscopy and Imaging during Focal Changes in Cerebral Hemodynamics

David A. Boas,*† Tom Gaudette,* Gary Strangman,* Xuefeng Cheng,†
John J. A. Marota,* and Joseph B. Mandeville*

*NMR Center, Massachusetts General Hospital, Harvard Medical School, Charlestown, Massachusetts 02129; and

†Electro-Optic Technology Center, Tufts University, Medford, Massachusetts 02155

Received January 21, 2000; published online November 7, 2000

Near infrared spectroscopy (NIRS) can detect changes in the concentrations of oxy-hemoglobin (HbO) and deoxy-hemoglobin (Hb) in tissue based upon differential absorption at multiple wavelengths. The common analysis of NIRS data uses the modified Beer-Lambert law, which is an empirical formulation that assumes global concentration changes. We used simulations to examine the errors that result when this analysis is applied to focal hemodynamic changes, and we performed simultaneous NIRS measurements during a motor task in adult humans and a neonate to evaluate the dependence of the measured changes on detector-probe geometry. For both simulations and *in vivo* measurements, the wide range of NIRS results was compared to an imaging analysis, diffuse optical tomography (DOT). The results demonstrate that relative changes in [HbO] and [Hb] cannot, in general, be quantified with NIRS. In contrast to that method, DOT analysis was shown to accurately quantify simulated changes in chromophore concentrations. These results and the general principles suggest that DOT can accurately measure changes in [Hb] and [HbO], but NIRS cannot accurately determine even relative focal changes in these chromophore concentrations. For the standard NIRS analysis to become more accurate for focal changes, it must account for the position of the focal change relative to the source and detector as well as the wavelength dependent optical properties of the medium. © 2001 Academic Press

INTRODUCTION

Optical methods based upon differential absorption proportional to concentrations of oxy-hemoglobin ([HbO]) and deoxy-hemoglobin ([Hb]) have long been applied to biological applications. Pulse oximetry non-invasively monitors arterial oxygen saturation by measuring arterial pulsation (1,2). Near infrared spectroscopy (NIRS) was developed to measure average tissue hemoglobin oxygen saturation and total hemoglobin

concentration (3–6). NIRS has been applied to such diverse applications as fundamental studies of brain function (7), neonate ECMO (8), and cardiac surgery (9) and we use it in this paper to refer to spectroscopic measurements made with a single source-detector pair. Diffuse optical tomography (DOT), a more recent technique (10), reconstructs images of changes in chromophore concentrations using multiple light sources and detectors. Both NIRS and DOT measure total optical absorption at multiple wavelengths, rather than differential absorption due to pulsation, and thus are sensitive to hemoglobin in the arterial, venial, and capillary compartments.

The ultimate promise of optical methodologies is simultaneous quantification of concentrations of multiple chromophores in order to determine changes in biologically relevant quantities like blood oxygen saturation and blood volume. Qualitative assessments severely limit the biological issues that can be addressed. For instance, a change in local [Hb] during stroke (11) or stimulus-induced brain activation (12,13), as measured by fMRI, can indicate a change in blood volume, oxygen saturation, or some combination of these possibilities.

Although it has generally been presumed that the biochemical specificity of optical absorption in the near infrared regime translates directly into quantifiable measurements of chromophore concentrations, the physics of optical methods merits increased attention as NIRS and DOT find increased application in biological systems. It has recently been shown that the common analysis of optical reflectance spectra from microscopic measurements introduces systematic “crosstalk” between calculated changes in [Hb] and [HbO] due to wavelength-dependent changes in optical pathlength during global brain activation (14). Corrections for this error may affect basic interpretations of physiology (e.g., 15). In this report, we address another fundamental issue: namely, can spectroscopic methods accurately determine relative changes in [Hb] and [HbO] during focal or graded hemodynamics changes, or are

imaging methods required to accurately measure these changes?

In order to address this issue, we illustrate the wide range of results that can be obtained by NIRS using the modified Beer–Lambert law, MBL (4,5), to calculate changes in [Hb] and [HbO] during focal motor activation in adult humans and a neonate. We then present a theoretical analysis of the accuracy of the modified Beer–Lambert law for quantifying focal concentration changes. We show that the wide disparity of results in interpreting human subject data using the MBL is consistent with our description of the errors being driven by partial volume and differential sensitivity effects. These errors can be significantly reduced by DOT (16,17).

THEORY

To set the theoretical context for our analysis, we briefly review the modified Beer–Lambert law as applied to quantifying global changes in oxy- and deoxyhemoglobin. The rest of the paper examines the validity of applying this simple theoretical model to analyzing focal changes.

Near-Infrared Spectroscopy

The theory of the modified Beer–Lambert Law (MBLL) has been explained previously (4,5). Briefly, the technique is based on the absorption of near infrared light by oxy- and deoxyhemoglobin. Changes in the concentrations of these chromophores are quantified using a modified Beer–Lambert law, which is an empirical description of optical attenuation in a highly scattering medium (4,5). The modified Beer–Lambert law is

$$\text{OD} = -\log \frac{I}{I_0} = \epsilon CLB + G, \quad (1)$$

where OD is the optical density, I_0 is the incident light intensity, I is the detected light intensity, ϵ is the extinction coefficient of the chromophore, C is the concentration of the chromophore, L is the distance between where the light enters the tissue and where the detected light exits the tissue, B is a pathlength factor, which accounts for increases in the photon pathlength caused by tissue scattering, and G is a factor which accounts for the measurement geometry. We use the convention of log base e .

A change in the chromophore concentration causes the detected intensity to change. When the concentration changes, the extinction coefficient ϵ and distance L remain constant and it is assumed that B and G remain constant. Thus, Eq. (1) can be rewritten as

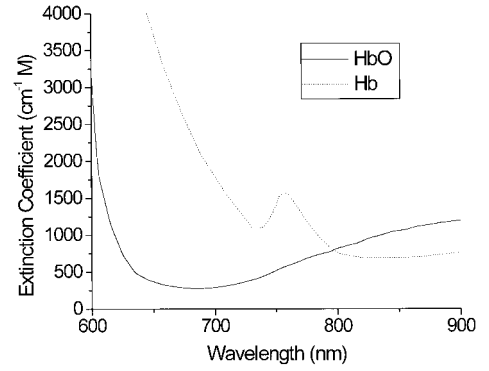


FIG. 1. These values for the molar extinction coefficients are in units of $[\text{cm}^{-1}/(\text{moles/liter})]$ and were obtained from (5,19,20).

$$\Delta\text{OD} = -\log \frac{I_{\text{Final}}}{I_{\text{Initial}}} = \epsilon \Delta CLB, \quad (2)$$

where $\Delta\text{OD} = \text{OD}_{\text{Final}} - \text{OD}_{\text{Initial}}$ is the change in optical density I_{final} and I_{Initial} are the measured intensities before and after the concentration change, and ΔC is the change in concentration. L is specified by the probe geometry, ϵ is an intrinsic property of the chromophore, and B is often referred to as the differential pathlength factor (DPF) and can be determined from independent measurements with ultrashort pulses of light (18) and has been tabulated for various tissues. Thus, given the extinction coefficient, it is possible to quantify the change in chromophore concentration.

Figure 1 plots the extinction coefficients for oxy- and deoxyhemoglobin versus wavelength as measured by Cope *et al.* (5,19,20). The wavelength range of 600 to 900 nm in the graph is the only region in which light is able to penetrate several centimeters through tissue. The other chromophores of significance in tissue in this wavelength range are water, lipids, and cytochrome aa3. We do not consider these chromophores in this paper, as their contribution in general is an order of magnitude less significant than hemoglobin. In order to consider the contribution of two chromophores, we must rewrite Eq. (2) as

$$\Delta\text{OD}^\lambda = (\epsilon_{\text{HbO}}^\lambda \Delta[\text{HbO}] + \epsilon_{\text{Hb}}^\lambda \Delta[\text{Hb}]) B^\lambda L, \quad (3)$$

where λ indicates a particular wavelength. Equation (3) explicitly accounts for independent concentration changes in oxyhemoglobin ($\Delta[\text{HbO}]$) and deoxyhemoglobin ($\Delta[\text{Hb}]$).

By measuring ΔOD at two wavelengths (λ_1 and λ_2) and using the known extinction coefficients of oxyhemoglobin (ϵ_{HbO}) and deoxyhemoglobin (ϵ_{Hb}) at those wavelengths, we can then determine the concentration changes of oxyhemoglobin and deoxyhemoglobin,

$$\begin{aligned}\Delta[\text{Hb}] &= \frac{\epsilon_{\text{HbO}}^{\lambda_2} \frac{\Delta\text{OD}^{\lambda_1}}{B^{\lambda_1}} - \epsilon_{\text{HbO}}^{\lambda_1} \frac{\Delta\text{OD}^{\lambda_2}}{B^{\lambda_2}}}{(\epsilon_{\text{Hb}}^{\lambda_1} \epsilon_{\text{HbO}}^{\lambda_2} - \epsilon_{\text{Hb}}^{\lambda_2} \epsilon_{\text{HbO}}^{\lambda_1})L} \\ \Delta[\text{HbO}] &= \frac{\epsilon_{\text{Hb}}^{\lambda_1} \frac{\Delta\text{OD}^{\lambda_2}}{B^{\lambda_2}} - \epsilon_{\text{Hb}}^{\lambda_2} \frac{\Delta\text{OD}^{\lambda_1}}{B^{\lambda_1}}}{(\epsilon_{\text{Hb}}^{\lambda_1} \epsilon_{\text{HbO}}^{\lambda_2} - \epsilon_{\text{Hb}}^{\lambda_2} \epsilon_{\text{HbO}}^{\lambda_1})L}.\end{aligned}\quad (4)$$

The generalization of this formula for more than two wavelengths can be found in (5).

Photon Diffusion Equation

A more rigorous theory for the migration of photons through tissue has been developed based on the radiative transport equation. This approach recognizes that near-infrared photons in tissue essentially undergo a random walk because the scattering probability is much greater than the absorption probability, and therefore their propagation through tissue can be described by a diffusion equation. The photon diffusion equation is (21–23),

$$-D\nabla^2\Phi(\mathbf{r}, t) + v\mu_a\Phi(\mathbf{r}, t) + \frac{\partial\Phi(\mathbf{r}, t)}{\partial t} = \mathbf{v}\mathbf{S}(\mathbf{r}, t).\quad (5)$$

$\Phi(\mathbf{r}, t)$ is the photon fluence at position \mathbf{r} and time t (the photon fluence is proportional to the intensity). $\mathbf{S}(\mathbf{r}, t)$ is the source distribution of photons. $D = v/(3\mu'_s)$ is the photon diffusion coefficient (24,25), μ'_s is the reduced scattering coefficient, μ_a is the absorption coefficient, and v is the speed of light in the medium. Note that the absorption coefficient is related to the extinction coefficient and the concentration as $\mu_a = \epsilon C$. For a combination of the hemoglobin chromophores,

$$\mu_a = \epsilon_{\text{HbO}}[\text{HbO}] + \epsilon_{\text{Hb}}[\text{Hb}].\quad (6)$$

Equation (5) accurately models the migration of light through highly scattering media provided that the probability of scattering is much greater than the absorption probability. Note that all factors in Eq. (5) are wavelength-dependent.

Solutions of the photon diffusion equation can be used to predict the photon fluence (or intensity) detected for typical diffuse measurements (23). Assuming that concentration changes are both global and small, the solution of the photon diffusion equation for a semi-infinite medium is

$$\begin{aligned}\Delta\text{OD} &= -\log \frac{\Phi_{\text{Final}}}{\Phi_{\text{Initial}}} \\ &= \frac{1}{2} \left(\frac{3\mu'_s}{\mu_a^{\text{Initial}}} \right)^{1/2} \left[1 - \frac{1}{(1 + L(3\mu'_s{}^{\text{Initial}}\mu_a^{\text{Initial}})^{1/2})} \right] \\ &\quad \times (\epsilon_{\text{HbO}}\Delta[\text{HbO}] + \epsilon_{\text{Hb}}\Delta[\text{Hb}])L.\end{aligned}\quad (7)$$

The solution of the photon diffusion equation for representative tissue geometry (Eq. (7)) tells us that the modified Beer–Lambert law is reasonable for tissues with spatially uniform optical properties when the chromophore concentration does not change significantly (i.e., $\Delta[X]/[X] \ll 1$). Equation (7) shows that the pathlength factor B in Eq. (3) is given by

$$B = \frac{1}{2} \left(\frac{3\mu'_s}{\mu_a^{\text{Initial}}} \right)^{1/2} \left[1 - \frac{1}{(1 + L(3\mu'_s{}^{\text{Initial}}\mu_a^{\text{Initial}})^{1/2})} \right]\quad (8)$$

for a semi-infinite medium. This shows that B depends on tissue scattering, initial chromophore concentration, extinction coefficient (and thus B is wavelength dependent), and optode separation. In practice, the validity of the assumption that B is independent of μ_a and L has often been ignored since B is in general empirically determined and the changes in μ_a are typically small. The validity of the approximation that changes in the optical properties are spatially uniform has not been checked. In particular, do systematic errors result when there is a focal change in the absorption coefficient, as during the cerebral vascular response to neural activity or ischemic stroke?

Diffuse Optical Tomography

In order to reconstruct an image of spatial variations in Hb and HbO, we need to measure $\Phi_{\text{sc}}(\mathbf{r}_d)$ at multiple source and detector positions and essentially back-project the image. The general solution of the photon diffusion equation for a medium with spatially varying absorption is

$$\begin{aligned}\Phi(\mathbf{r}_d) &= \Phi_{\text{incident}}(\mathbf{r}_d) - \int \Phi(\mathbf{r}) \frac{v}{D} (\epsilon_{\text{HbO}}\Delta[\text{HbO}] \\ &\quad + \epsilon_{\text{Hb}}\Delta[\text{Hb}])G(\mathbf{r}, \mathbf{r}_d) d\mathbf{r}.\end{aligned}\quad (9)$$

For reflectance in a semi-infinite medium, the solutions for Φ_{incident} and $G(\mathbf{r}, \mathbf{r}_d)$ can be found in Farrell *et al.* (26). Equation (9) is an implicit equation for the measured fluence as $\Phi(\mathbf{r})$ appears in the integral on the right-hand-side. This equation can be solved using the first Born approximation, which assumes that $\Phi(\mathbf{r}) = \Phi_{\text{incident}} + \Phi_{\text{sc}}$ where (27,28)

$$\Phi_{sc}(\mathbf{r}_d) = - \int \Phi_{incident}(\mathbf{r}) \frac{v}{D} (\epsilon_{HbO} \Delta[\text{HbO}] + \epsilon_{Hb} \Delta[\text{Hb}]) G(\mathbf{r}, \mathbf{r}_d) d\mathbf{r}. \quad (10)$$

By measuring $\Phi_{sc}(\mathbf{r}_d)$ using multiple source and detector positions and multiple wavelengths, we can invert the integral equation to obtain images of $\Delta[\text{HbO}]$ and $\Delta[\text{Hb}]$. There are numerous methods for solving Eq. (10) (29). Most rely on reducing Eq. (10) to a matrix equation by rewriting the integral as a sum over voxels, i.e., $y = Ax$, where y is the vector of measurements $\Phi_{sc}(\mathbf{r}_d)$, x is the vector of image voxels, and A is the transformation matrix obtained from the integrand of Eq. (10). The integrand of Eq. (10) essentially describes the sensitivity that each measurement has to the change in absorption within each volume element within the medium. In other words, if the absorption changes within a localized region, then

$$\begin{aligned} \Delta OD_{\text{BORN}} &= -\log\left(\frac{\Phi_{incident}(\mathbf{r}_s, \mathbf{r}_d) + \Phi_{sc}(\mathbf{r}_s, \mathbf{r}_d)}{\Phi_{incident}(\mathbf{r}_s, \mathbf{r}_d)}\right) \\ &\approx -\frac{\Phi_{sc}(\mathbf{r}_s, \mathbf{r}_d)}{\Phi_{incident}(\mathbf{r}_s, \mathbf{r}_d)} = \frac{\Phi_{incident}(\mathbf{r}_s, \mathbf{r}) G(\mathbf{r}, \mathbf{r}_d) v d\mathbf{r}}{\Phi_{incident}(\mathbf{r}_s, \mathbf{r}_d) D} \Delta\mu_a, \end{aligned} \quad (11)$$

where $d\mathbf{r}$ is the volume over which the absorption change $\Delta\mu_a$ occurs and $\Delta\mu_a^\lambda = (\epsilon_{HbO}^\lambda \Delta[\text{HbO}] + \epsilon_{Hb}^\lambda \Delta[\text{Hb}])$.

Hemodynamic Cross-Talk Resulting from a Systematic Error

When we use the modified Beer–Lambert law (Eq. (3)) to analyze the absorption change within a focal region (Eq. (11)), we are assuming that $\Delta OD_{\text{MBLL}}^\lambda = \Delta OD_{\text{BORN}}^\lambda$. This gives us

$$\begin{aligned} \Delta\mu_{a,\text{MBLL}}^\lambda &= \frac{1}{B^\lambda L} \frac{\Phi_{incident}(\mathbf{r}_s, \mathbf{r}) G^\lambda(\mathbf{r}, \mathbf{r}_d) v d\mathbf{r}}{\Phi_{incident}(\mathbf{r}_s, \mathbf{r}_d) D} \\ &\quad \times \Delta\mu_{a,\text{BORN}}^\lambda = k^\lambda \Delta\mu_{a,\text{BORN}}^\lambda. \end{aligned} \quad (12)$$

$\Delta\mu_{a,\text{BORN}}^\lambda$ is the real change in absorption ($\Delta\mu_{a,\text{Real}}^\lambda$) and $\Delta\mu_{a,\text{MBLL}}^\lambda$ is the absorption change that we will measure ($\Delta\mu_{a,\text{Meas}}^\lambda$) having assumed the accuracy of the modified Beer–Lambert Law. This indicates that we will misestimate the real absorption change by k^λ . k^λ will typically be less than 1 due to the partial volume effect.

To explore the effect of this factor on our determination of $\Delta[\text{HbO}]$ and $\Delta[\text{Hb}]$, we return to Eq. (4) which related the measured concentration changes to the measured absorption changes:

$$\begin{aligned} \Delta[\text{Hb}]_{\text{Meas}} &= \frac{\epsilon_{HbO}^{\lambda_2} k^{\lambda_1} \Delta\mu_{a,\text{REAL}}^{\lambda_1} - \epsilon_{HbO}^{\lambda_1} k^{\lambda_2} \Delta\mu_{a,\text{REAL}}^{\lambda_2}}{(\epsilon_{Hb}^{\lambda_1} \epsilon_{HbO}^{\lambda_2} - \epsilon_{Hb}^{\lambda_2} \epsilon_{HbO}^{\lambda_1})} \\ &= \frac{\epsilon_{HbO}^{\lambda_1} \epsilon_{HbO}^{\lambda_2} (k^{\lambda_1} - k^{\lambda_2}) \Delta[\text{HbO}]_{\text{Real}} - (k^{\lambda_1} \epsilon_{Hb}^{\lambda_1} \epsilon_{HbO}^{\lambda_2} - k^{\lambda_2} \epsilon_{Hb}^{\lambda_2} \epsilon_{HbO}^{\lambda_1}) \Delta[\text{Hb}]_{\text{Real}}}{(\epsilon_{Hb}^{\lambda_1} \epsilon_{HbO}^{\lambda_2} - \epsilon_{Hb}^{\lambda_2} \epsilon_{HbO}^{\lambda_1})} \quad (13) \\ \Delta[\text{HbO}]_{\text{Meas}} &= \frac{\epsilon_{Hb}^{\lambda_1} k^{\lambda_2} \Delta\mu_{a,\text{REAL}}^{\lambda_2} - \epsilon_{Hb}^{\lambda_2} k^{\lambda_1} \Delta\mu_{a,\text{REAL}}^{\lambda_1}}{(\epsilon_{Hb}^{\lambda_1} \epsilon_{HbO}^{\lambda_2} - \epsilon_{Hb}^{\lambda_2} \epsilon_{HbO}^{\lambda_1})} \\ &= \frac{(k^{\lambda_2} \epsilon_{Hb}^{\lambda_1} \epsilon_{HbO}^{\lambda_2} - k^{\lambda_1} \epsilon_{Hb}^{\lambda_2} \epsilon_{HbO}^{\lambda_1}) \Delta[\text{HbO}]_{\text{Real}} - \epsilon_{Hb}^{\lambda_1} \epsilon_{Hb}^{\lambda_2} (k^{\lambda_1} - k^{\lambda_2}) \Delta[\text{Hb}]_{\text{Real}}}{(\epsilon_{Hb}^{\lambda_1} \epsilon_{HbO}^{\lambda_2} - \epsilon_{Hb}^{\lambda_2} \epsilon_{HbO}^{\lambda_1})}. \end{aligned}$$

If the measurements at different wavelengths have the same sensitivity to the focal change, then $k^{\lambda_1} = k^{\lambda_2}$ and Eq. (13) reduces to $\Delta[X]_{\text{Meas}} = k \Delta[X]_{\text{Real}}$ such that the value we measure is linearly proportional to the correct value and the calculated ratio $\Delta[\text{HbO}]:\Delta[\text{Hb}]$ equals the correct ratio. However, since the optical properties at different wavelengths are generally different, the spatial sensitivity profiles are thus also expected to be different with the result that $k^{\lambda_1} \neq k^{\lambda_2}$. Therefore, in general, there is cross-talk between real focal hemoglobin concentration changes and the determined/calculated concentration changes. This cross-talk can only be removed if the values of k^{λ_1} and k^{λ_2} are known. This problem can potentially be solved by diffuse optical tomography, or prior knowledge of the geometry and optical properties of the head as well as the spatial location and extent of the focal activation. This paper explores the significance of this cross-talk in experiments and simulations.

METHODS

Adult Human Brain Activation

We compared signals recorded from neighboring detector fibers on an adult human during the performance of a simple motor task. The study was performed under a protocol approved by the MGH internal review board. A single source location was positioned 1.5 cm posterior to position C3 in the EEG 10-20 system. This source was composed of two laser diodes—780 and 830 nm—which were fed into a 1 mm bifurcated fiber. A 2-mm detector fiber was positioned 1.8 cm anterior to C3 (on the line formed by C3 and the source). Another detector fiber was also positioned 3.3 cm from the source, but more medially than the first detector, with a center-to-center detector separation of 1.0 cm. It has been shown that C3 and C4 lie approximately over the hand areas of primary motor cortex

(30). Hence, this optode arrangement was expected to sample M1 for the right hand.

Prior to commencing the recording, the subject was asked to simply rest quietly. When the experimental run began, the subject alternated between quiet rest for 15 s, and 15 s of 4-finger flexion/extension with the right hand (at approximately 3 Hz). The subject performed 10 blocks of the motor task, interleaved with 11 blocks of rest, for a total run length of 315 s.

Adult Human Data Analysis

The resulting motor-task data was time-trigger averaged—separately for each wavelength and detector—and triggering on the onset of motor activation. Thus, each data point in the four resulting timeseries is an average of 10 points in the original data. The two timeseries pairs (780 and 830 nm, for each of two detectors) were then analyzed using the modified Beer–Lambert law. This resulted in four new timeseries: Hb and HbO time-courses for each of the two detectors. For the pathlength factor B , a fixed value of 5.93 was used (31). To summarize the results across three subjects we averaged the concentration change for 5 s before onset of stimulation and then from 6–11 s following onset of the stimulus. The differences of these average values are compared.

Neonate Brain Activation

We compared a MBLL and DOT analysis of diffuse optical data obtained during a motor-sensory brain activation in a newborn human. All clinical studies were performed under a protocol approved by an institutional review board-, and parents signed informed consent prior to initiation of studies. More details of this human subject study can be found in Hintz *et al.* (36). For the results presented here, a 32–33 week EGA infant underwent a passive motor stimulation protocol. The infant was quiet and asleep, but not pharmacologically sedated. The patient had a normal heart rate and O_2 saturation by pulse oximetry during the approximately 40-min study period.

For this study, a large probe was designed and was placed in true midline position in the area that corresponded to the motor cortex (see Fig. 3). For the optical probe, the nine source fibers were arranged in a 3×3 grid with a 2×1 -cm spacing. The 16 collection fibers were arranged in a 4×4 grid with the same 2×1 -cm spacing. To improve optical coupling, the height of each fiber was manually adjusted to match the surface contours of the skull. The Z positions were not measured, nor was the actual contour of the scalp. There were no complications from probe placement.

Baseline data were collected for 20 s, then the patient's right arm was flexed and extended at the elbow with a 1 Hz repetition rate. This study employed a 5-s integration time, and each stimulation period was 30 s

with a rest period of 45–60 s between each stimulation period. Imaging data was collected at both 780 and 830 nm to facilitate a spectroscopic determination of oxy- and deoxyhemoglobin.

Neonate Data Analysis

The optical data recorded from the multiple source-detector pairs on the neonate brain was analyzed using two different approaches: a NIRS analysis was performed for each source-detector pair using the modified Beer–Lambert law (MBLL), and a DOT analysis combined the information from all such pairs to reconstruct images of optical absorption. Each analysis treated the geometry as a semi-infinite medium with a homogeneous distribution of absorbers, except for the localized activation, and used the expression presented previously. For the MBLL analysis, the pathlength factor B was calculated using Eq. (10) with $\mu'_s = 10.0 \text{ cm}^{-1}$, $[\text{HbT}] = 100 \text{ } \mu\text{M}$, $\text{SO}_2 = 85\%$, and the known separations L between various source-detector pairs.

For the DOT analysis, we used the Simultaneous Iterative Reconstruction Technique (SIRT) to invert Eq. (10) (17,28). SIRT is a variation of the Algebraic Reconstruction Technique (ART), which sequentially projects estimates onto a hyperplane defined by a particular row of the linear system. SIRT has been observed to generate smoother reconstructions of the object function due to the averaging over a number of projections, but this comes at a cost of slower convergence. The SIRT reconstruction can be expressed mathematically as $\hat{\mathbf{x}}_i = \hat{\mathbf{x}}_{i-1} - \text{mean}((\hat{\mathbf{x}}_{i-1}^T \mathbf{a}_j - b_j / (\mathbf{a}_j^T \mathbf{a}_j)) \mathbf{a}_j)$, where $\hat{\mathbf{x}}_i$ is the i^{th} estimate of the object function, \mathbf{a}_i is the i^{th} row of the transformation matrix A , and b_i is the i^{th} measurement. For underdetermined systems, this reconstruction will converge to a point on the hyperplane satisfying the linear system that is nearest to the initial guess. Limiting the number of interactions controls regularization; our reconstructions were performed using 10 iterations of the SIRT algorithm, starting with an initial guess of zero perturbation.

DOT images were reconstructed in a 6×3 -cm plane positioned at a depth of 1 cm, with a thickness of 3 mm, and located parallel to the source/detector plane. The voxel size was $3 \times 1.5 \times 3$ mm in the x , y , and z directions respectively, giving an image with $21 \times 21 \times 1$ voxels. With this geometry, we reconstructed 2-D images of the absorption coefficient, and we assumed that the out-of-plane optical properties remain unchanged. This means that any out-of-plane optical changes were projected into the image plane.

Simulations

In order to understand the wide range of results obtained by our simultaneous NIRS measurements in the neonate, we simulated the experimental setup and the process of light diffusion through a simplified me-

dium containing a focal hemodynamic change. The simulated data, based upon the forward solution to the diffusion equation, was analyzed using the MBLL and DOT methods described previously in order to determine how closely each method reconstructed the known changes in chromophore concentrations.

To simulate changes in the diffuse intensity (i.e., ΔOD) due to a focal change in total hemoglobin concentration, we employed the first Born approximation (Eq. (12)) to solve the photon diffusion equation. We used a reduced scattering coefficient of 10 cm^{-1} and included absorption coefficients at wavelengths of 780 and 830 nm that depended only upon oxy- and deoxyhemoglobin. To calculate the absorption coefficient for different concentrations of hemoglobin, we used the tabulated extinction coefficients provided by Cope *et al.* (5,19,20) as shown in Fig. 1. For the semi-infinite medium, we used an index of refraction $n = 1.33$, and we assumed baseline values of $\text{HbT} = 100 \mu\text{M}$ and $\text{SO}_2 = 85\%$ to give $\mu_a^{780} = 0.175 \text{ cm}^{-1}$ and $\mu_a^{830} = 0.214 \text{ cm}^{-1}$. A focal increase in absorption (the "object") was positioned half-way between the first source (S1) and sixth detector (D6) at a depth of 1 cm. It had dimensions of $0.3 \times 0.15 \times 0.3 \text{ mm}$ in x , y , and z respectively. The reduced scattering coefficient of the object was the same as the background, and the absorption coefficient was $\mu_a^{780} = 0.210 \text{ cm}^{-1}$ and $\mu_a^{830} = 0.257 \text{ cm}^{-1}$ corresponding to a 20% increase in total hemoglobin concentration and $\delta\mu_a^{780} = 0.035 \text{ cm}^{-1}$ and $\delta\mu_a^{830} = 0.043 \text{ cm}^{-1}$. The image of the change in the absorption coefficient was reconstructed with 10 iterations of SIRT, as described above for the neonate data analysis.

Numerous optical instruments available for measurements of localized concentration changes in general, and brain function specifically, utilize more than two wavelengths. The Hamamatsu NIRO-500 uses four wavelengths of 778, 813, 867, and 900 nm. A system developed by ISS uses 8 wavelengths of 631, 670, 751, 776, 786, 813, 830, and 841 nm (personal communication with Franceschini). True white-light spectroscopy systems also exist that utilize the whole wavelength spectrum from 700–900 nm for example (32). We have therefore also performed simulations on the above geometry using these three different wavelength combinations. Furthermore, in addition to a focal change of 20% in [HbO] and [Hb], we also considered a 30% decrease in [Hb] and a 29% increase in [HbO].

RESULTS

Adult NIRS

The results of the adult NIRS experiment appear in Fig. 2. The dark bar atop each graph indicates the time of motor activity (0–15 s). The oxyhemoglobin curves for the two detectors (bottom panel) lie directly atop

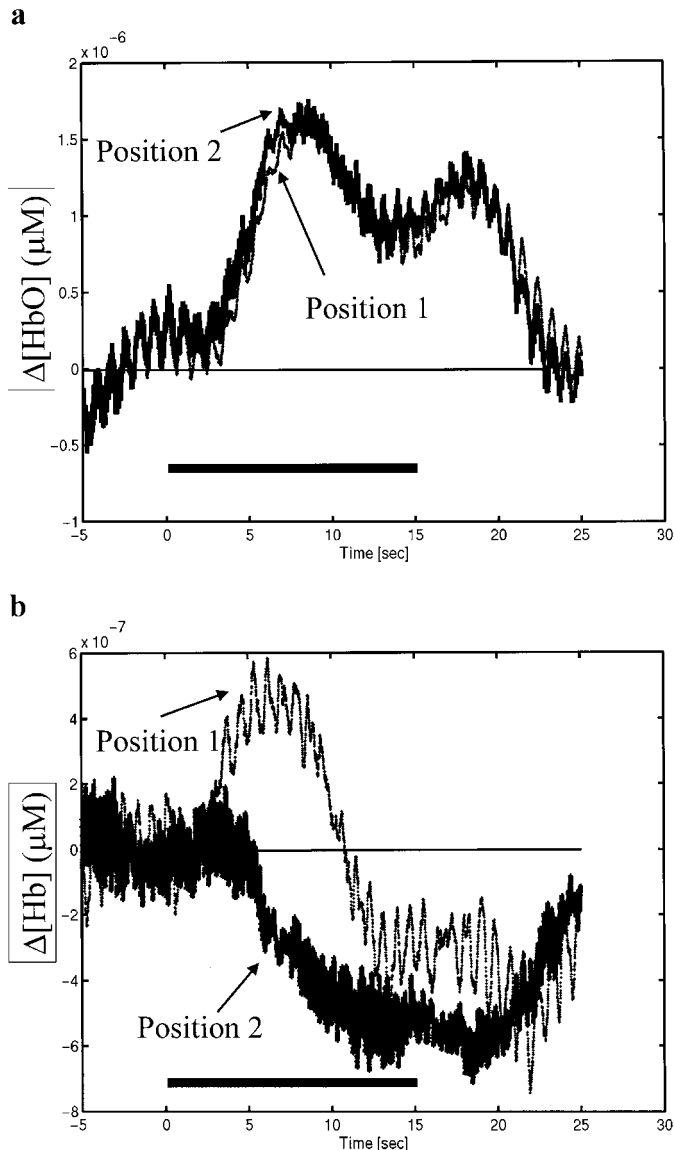


FIG. 2. Time course of $\Delta[\text{HbO}]$ and $\Delta[\text{Hb}]$ response to a motor stimulation lasting 15 s from $t = 0$ to 15 s. The response at the two different detectors are shown for the first subject. Notice that $\Delta[\text{Hb}]$ differs between the two detectors while $\Delta[\text{HbO}]$ remains nearly the same. In addition, the initial increase and peak in $\Delta[\text{Hb}]$ at position 1 is similar to that of $\Delta[\text{HbO}]$.

one another. Both exhibit an increase in [HbO] starting at approximately 3 s and peaking at approximately 8 s which, after the cessation of motor activity, decreases back to baseline in approximately 9 s. The deoxyhemoglobin curves, however, are not at all similar. One detector shows an early increase in Hb (3–10 s) that partially coincides with the [HbO] rise, whereas the other detector shows only a decrease in [Hb] starting around 5 s, peaking at 10 s, and returning to baseline around 25 s (that is, 10 s after cessation of motor activity). It is clear from these two graphs that the

TABLE 1

Summary of the Peak Response in $\Delta[\text{HbO}]$ and $\Delta[\text{Hb}]$ at the Two Different Detector Positions for Three Subjects

Subject	Position	$\Delta[\text{HbO}]$ (μM)	$\Delta[\text{Hb}]$ (μM)	$\Delta[\text{HbO}]/\Delta[\text{Hb}]$
A	#1	1.4	0.31	4.5
	#2	1.5	-0.36	-4.2
B	#1	0.46	8.1e-4	570
	#2	-0.21	1.0	-0.21
C	#1	1.3	0.067	19
	#2	1.1	0.16	6.9

$\Delta[\text{Hb}]/\Delta[\text{HbO}]$ ratio is not only different between the two detectors, but it is not even of the same sign.

Table 1 quantifies this lattermost phenomenon observed across three subjects. The first column shows $\Delta[\text{Hb}]$ and $\Delta[\text{HbO}]$ calculated by subtracting the mean of the prebaseline (-5 to 0 s) from the mean at the initial activation peaks (6 to 11 s). Using these numbers for the first subject, notice that the $\Delta[\text{HbO}]/\Delta[\text{Hb}]$ ratios for detector 1 would all turn out positive, while the same ratios are negative for detector 2, despite (assumed) overlapping brain sensitivity profiles given their relatively small (1 cm) separation. Similar large discrepancies are seen in the other two subjects.

Neonate

DOT images of the focal changes in absorption at 780 and 830 nm in response to 30 s of the sensory motor stimulation in the neonate are shown in Fig. 3. The images were obtained by averaging 5 different stimulation trials on a single neonate. The transition from blue to green to red indicates increasing absorption on a linear scale indicated by the color bar. These images indicate a focal increase in the total hemoglobin concentration, which is consistent with an increase in blood flow to the activated region in the contralateral cortex. A region of interest analysis of the activated region in the contralateral cortex indicated that $\Delta[\text{Hb}] = 2.8 \mu\text{M}$ and $\Delta[\text{HbO}] = 8.5 \mu\text{M}$.

An overlay of the sources and detectors on the DOT absorption image obtained at 780 nm is shown in Fig. 4a. The changes in oxy- and deoxyhemoglobin as determined by MBLL analyses for source S7 with detectors D1, D2, D5, and D6 are shown in Fig. 4b together with the result obtained using the DOT analysis. Note that absolute changes in $[\text{Hb}]$ and $[\text{HbO}]$ as determined by the MBLL were more than an order of magnitude smaller than the DOT result; this difference was expected and is trivially explained as a partial volume error arising from the focal nature of the hemodynamic

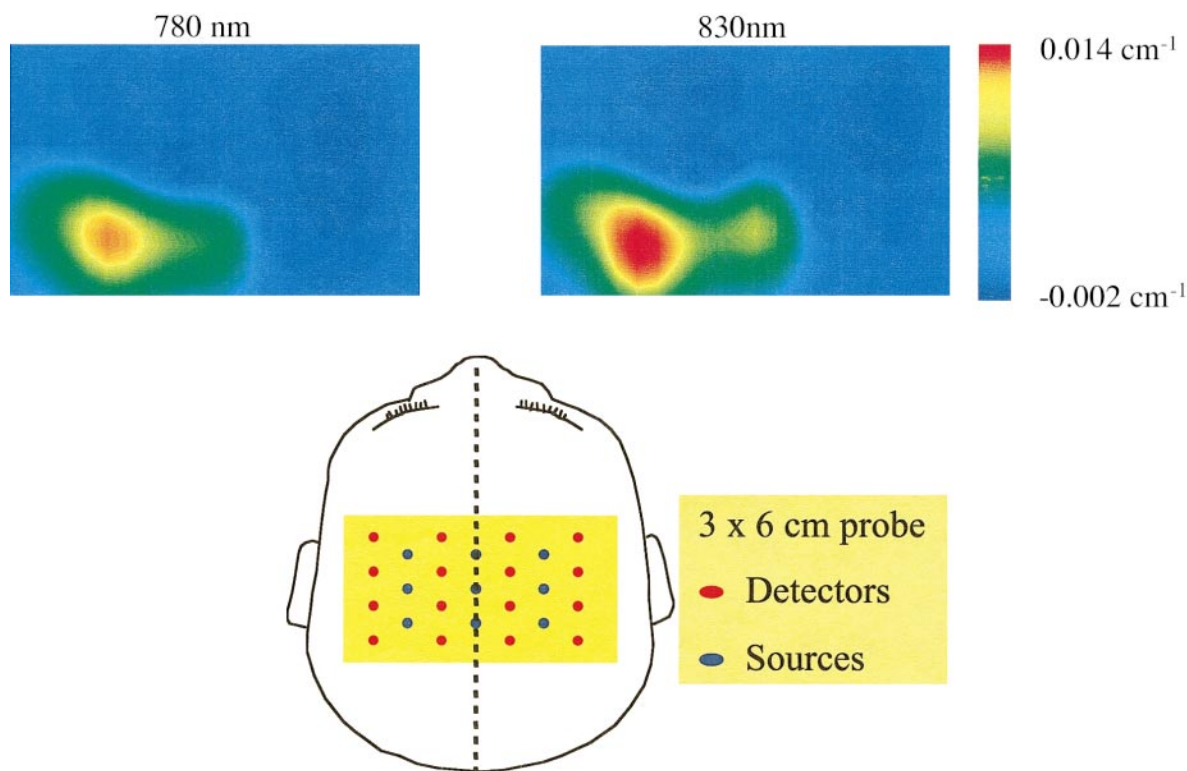


FIG. 3. Diffuse optical tomography images obtained from activation of the motor-sensory cortex of a neonate. The drawing of the neonate head indicates the position of the sources and detectors on the scalp. In the images, which were reconstructed in a plane parallel to the plane of sources and detectors, red indicates an increase in the absorption coefficient while blue indicates a small decrease in the absorption coefficient due to the activation. Images are shown for the measurements made at 780 and 830 nm.

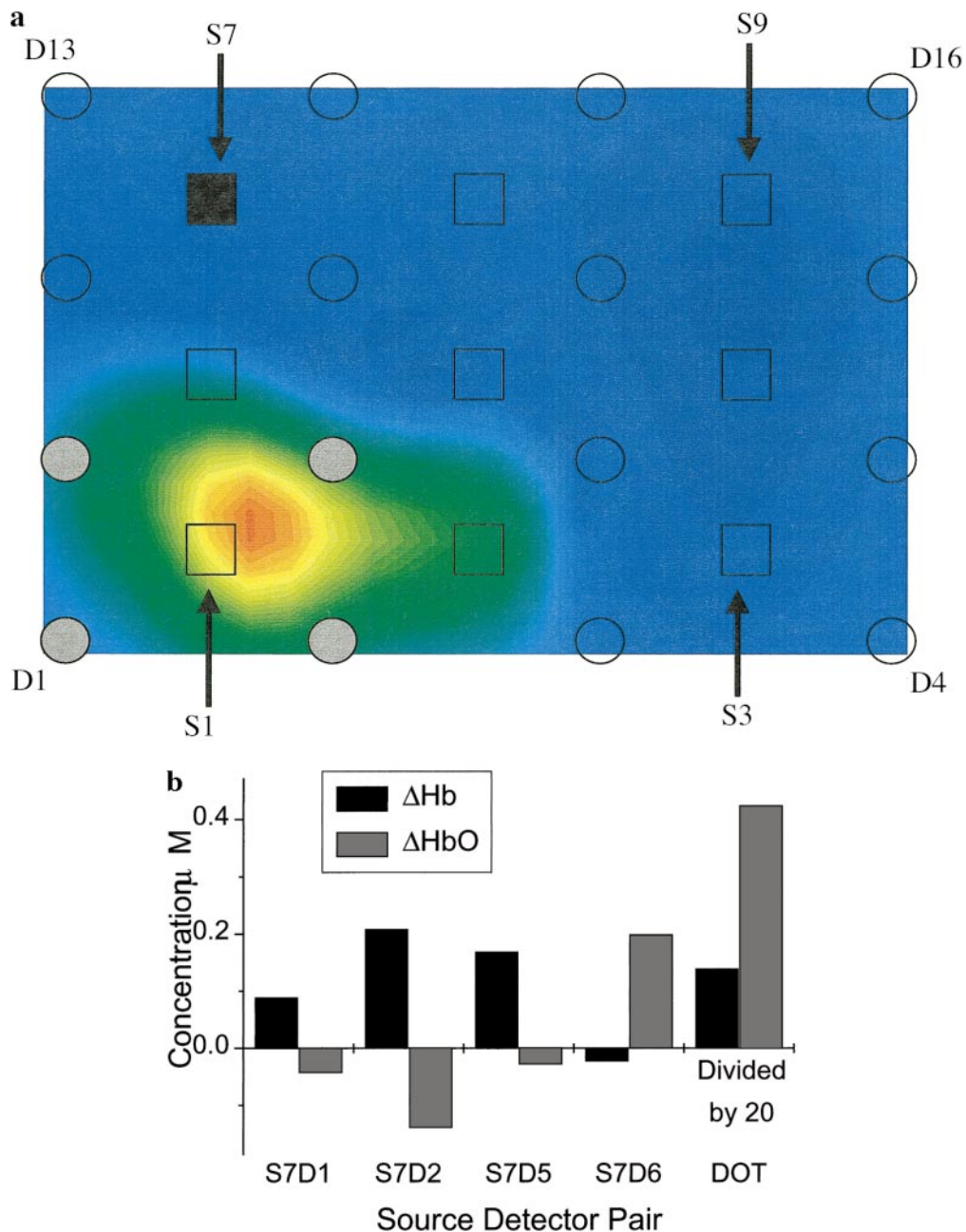


FIG. 4. (a) An overlay of the sources and detectors on the image reconstructed at 780 nm. (b) NIRS analysis of the measurements made between source 7 and detectors 1, 2, 5, and 6. The calculated changes in [HbO] and [Hb] reveal significant differences depending on the position of the detector. The result obtained by DOT is shown of the right (its magnitude has been reduced by 20-fold).

response. More significantly, however, the MBLL analyses for each source-detector pair determined widely different relative changes in [Hb] in [HbO], even though the source and all detectors were in close proximity to the focal hemodynamic alteration as determined by DOT.

Simulations

The image reconstructed from the simulation at 780 nm is presented in Fig. 5a with an overlay indicating

the positions of the sources and detectors. The color scale is linear with the transition from blue to green to red indicating an increased absorption. Note that the centroid of the reconstructed object was shifted toward source S1 relative to the actual location, which is marked on the figure with an "X". The full width at half maximum of the reconstructed object was significantly larger than the real object due to a point spread function introduced by the probabilistic nature of photon diffusion and the limited sampling. However, the re-

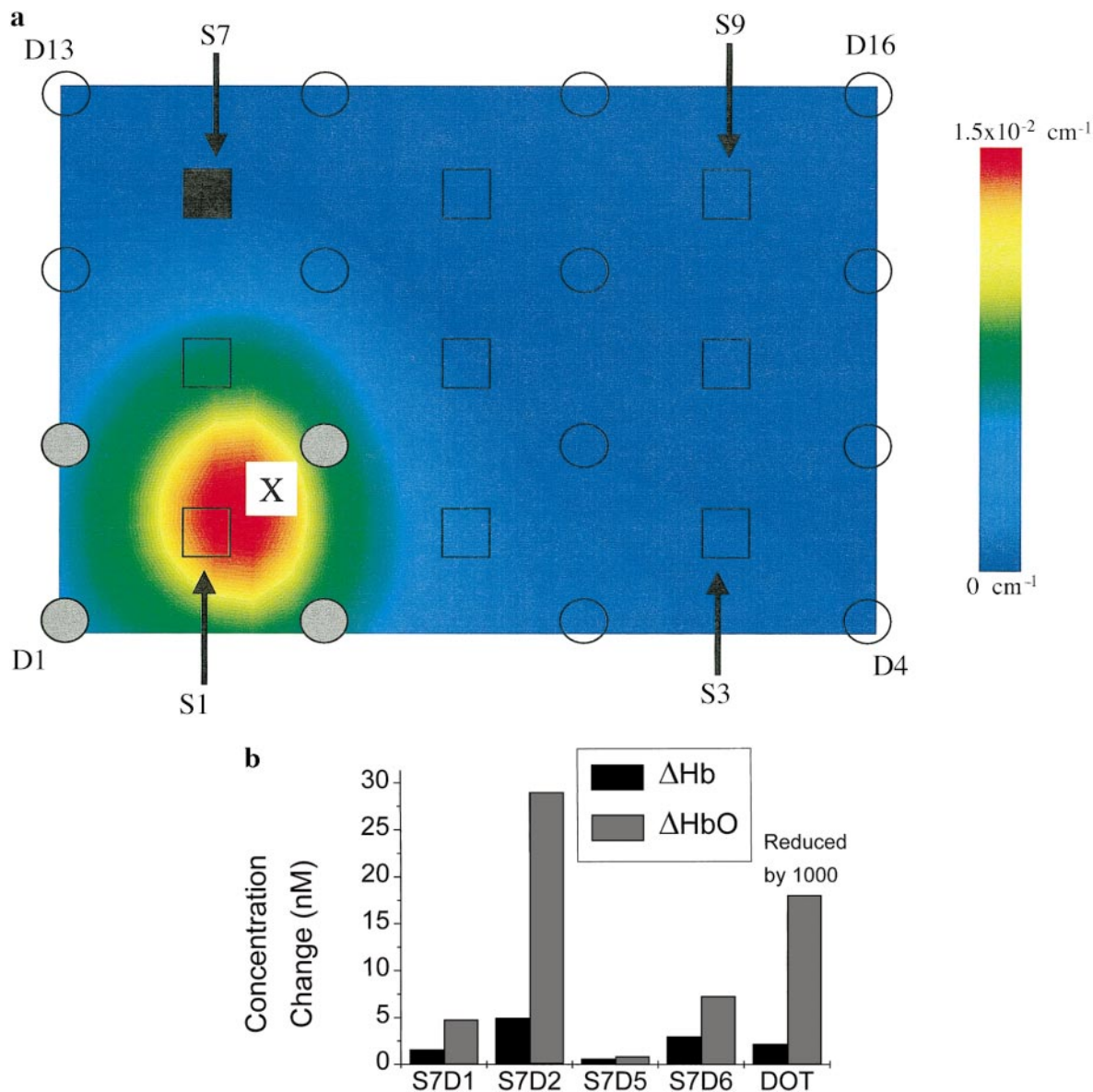


FIG. 5. (a) An overlay of the sources and detectors on the image reconstructed at 780 nm from simulated data. The “x” near source 1 reveals the actual position of the absorbing object. The DOT reconstruction resulted in $\Delta[HbO] = 17 \mu\text{M}$ and $\Delta[Hb] = 3.0 \mu\text{M}$ compared to the actual values of $\Delta[HbO] = 17 \mu\text{M}$ and $\Delta[Hb] = 3.0 \mu\text{M}$. (b) NIRS analysis of the measurements made between source 7 and detectors 1, 2, 5, and 6. The calculated changes in $[HbO]$ and $[Hb]$ are 3 orders of magnitude smaller than the actual changes and reveal significant differences depending on the position of the detector. For comparison, the DOT result is shown on the right, reduced by 3 orders of magnitude. The DOT result agrees well with the actual result.

constructed peak change in the absorption coefficient was approximately equal to the known change. The image at 830 nm was similar. A region of interest analysis using a 3 by 3 voxel square centered around the peak absorption revealed that the reconstructed object had $\Delta[Hb] = 2.2 \mu\text{M}$ and $\Delta[HbO] = 18 \mu\text{M}$, which is similar to the actual changes of $\Delta[Hb] = 3.0 \mu\text{M}$ and $\Delta[HbO] = 17 \mu\text{M}$. As expected, the magnitude of these changes diminished using larger summated regions due to the focal nature of the hemodynamic perturbation, but the ratio of $\Delta[Hb]$ to $\Delta[HbO]$ was less

sensitive to the region size because images of $\Delta[Hb]$ and $\Delta[HbO]$ were blurred in similar ways by the reconstruction.

Figure 5b presents the MBL analysis of the simulated data as determined for source S7 with detectors D1, D2, D5, and D6. In terms of absolute quantification of $\Delta[Hb]$ and $\Delta[HbO]$, the MBL results were more than 3 orders of magnitude smaller than the known changes. The results obtained at detectors D1 and D2 were much larger than found at detectors D5 and D6 because a larger fraction of the light detected at the

former detectors sampled the object. We tested how these results changed as $\Delta[\text{HbT}]$ increased from 10 to 50 μM at constant oxygen saturation, and we found linear relationships between changes in $\Delta[\text{Hb}]$ and $\Delta[\text{HbO}]$ for each source-detector pair. However, the linear slopes were widely different for each source-detector pair, as illustrated for the single value of $\Delta[\text{HbT}]$ analyzed and presented in Fig. 5b.

Although it was expected that a MBLL analysis should reduce the absolute magnitudes of measured concentration changes when applied to a focal change, the more significant result was that the MBLL did not even preserve the relative magnitudes of $\Delta[\text{Hb}]$ and $\Delta[\text{HbO}]$. The full extent of this problem is illustrated in Fig. 6a, which displays the $\Delta[\text{HbO}]/\Delta[\text{Hb}]$ ratio obtained by a MBLL analysis of the simulated data for each possible combination of the 16 detectors and 9 sources. While the known ratio is 5.7, the MBLL ratios range from less than 0 to 11. The four source-detector pairs that agree best with the correct value are circled and correspond to source-detector pairs S4D1, S4D3, S7D3, and S9D2.

The wide range of $\Delta[\text{HbO}]/\Delta[\text{Hb}]$ ratios can be understood in terms of the differential sensitivities of each wavelength to the region of the focal object. From Eq. (10) we calculated the sensitivity to the focal absorbing region for each source-detector measurement at each wavelength. Figure 6b shows the ratio of the sensitivity at 780 nm to that at 830 nm for each source-detector pair. When the sensitivity at each wavelength was the same (and thus the ratio of sensitivities is 1), calculated ratios of $\Delta[\text{HbO}]$ and $\Delta[\text{Hb}]$ agreed with the actual ratio. The four source-detector pairs for which the sensitivity ratio was closest to 1 are circled in Fig. 6b; this is more clearly illustrated in the expanded color scale shown in Fig. 6c. Comparison with Fig. 6a demonstrates that these source-detector pairs are the same pairs that produce the most accurate evaluation of the true $[\text{HbO}]:[\text{Hb}]$ ratio.

Finally, Fig. 6d graphs the $\Delta[\text{HbO}]/\Delta[\text{Hb}]$ ratio versus the ratio of 730 nm sensitivity to 830 nm sensitivity. Each data point in this figure corresponds to one of the 144 measurements with the 16 detectors and 9 sources. This graph reveals the strong dependence of the calculated ratio on the differential wavelength sensitivity. A $\pm 20\%$ difference in wavelength sensitivity causes a 50 to 100% systematic error in the relative values of $\Delta[\text{HbO}]$ and $\Delta[\text{Hb}]$. If the measurement at 830 nm is more sensitive to the volume of the focal change than that at 780 nm, then $\Delta[\text{HbO}]$ will be overestimated relative to $\Delta[\text{Hb}]$. This occurs because the extinction coefficient at 830 nm is more sensitive to changes in $[\text{HbO}]$ than $[\text{Hb}]$. The reverse occurs if the measurement at 780 nm is more sensitive to the focal volume. It is interesting to note that even the sign of $\Delta[\text{HbO}]/\Delta[\text{Hb}]$ changes if the sensitivity at 780 nm becomes significantly greater than that at 830 nm.

The results of simulations exploring the effect of using more wavelengths and different concentration changes is summarized in Fig. 7. Basically, increasing the number of wavelengths used in the measurement can decrease the systematic error, but it can also increase the error. In addition, the magnitude of the fractional error in the ratio $\Delta[\text{HbO}]/\Delta[\text{Hb}]$ depends on the real concentration changes in the focal region.

DISCUSSION

In this study, we observed a wide variance in the MBLL results for multiple simultaneous acquisitions during a motor task in adult humans and a neonate. MBLL and DOT results did not agree in terms of absolute magnitudes, relative magnitudes, or even the relative sign for changes in $[\text{HbO}]$ and $[\text{Hb}]$. In order to investigate sources of error in chromophore quantification by using the standard modified Beer-Lambert Law (MBLL) analysis of NIRS data, we performed a simplified optical simulation using a similar geometry to the *in vivo* study. The *in vivo* data, the results of the optical simulation, and the underlying principles suggest that the standard MBLL analysis cannot accurately quantify even relative changes in $\Delta[\text{HbO}]$ and $\Delta[\text{Hb}]$ for a hemodynamic perturbation that is focal in nature, whereas DOT can produce a much more accurate representation of hemodynamic changes. DOT is less susceptible to such errors as it accounts for spatial variation in the changes by proper analysis of multiple overlapping measurements spanning the region. It may be possible to obtain better results from the NIRS data by using an analysis method that accounts for the spatial variation, as opposed to the MBLL.

One standard approach to minimizing the variation in the MBLL analysis of NIRS data from brain activation, has been to position the source and detector so as to maximize the measured signal. In this way the partial-volume effect is minimized and the results are believed to be accurate. However, our results show that adjusting the optodes to maximize the signal (ΔOD) does not necessarily produce results with the correct ratio $\Delta[\text{HbO}]/\Delta[\text{Hb}]$. Importantly, it does appear that following this procedure does insure the proper sign for the concentration changes even though the relative magnitudes are inaccurate.

In the human, focal brain activation was localized by repeated placement of the optodes to maximize the recorded activation signal. Our MBLL analysis of the NIRS data obtained absolute magnitudes for $\Delta[\text{HbO}]$ and $\Delta[\text{Hb}]$ that showed a wide variance between different source-detector pairs. This result could be explained simply as a partial volume error arising from the focal nature of the brain activation, since the partial volume error will depend upon the geometry between source, detector, and activated region. However, a more surprising and significant observation was that

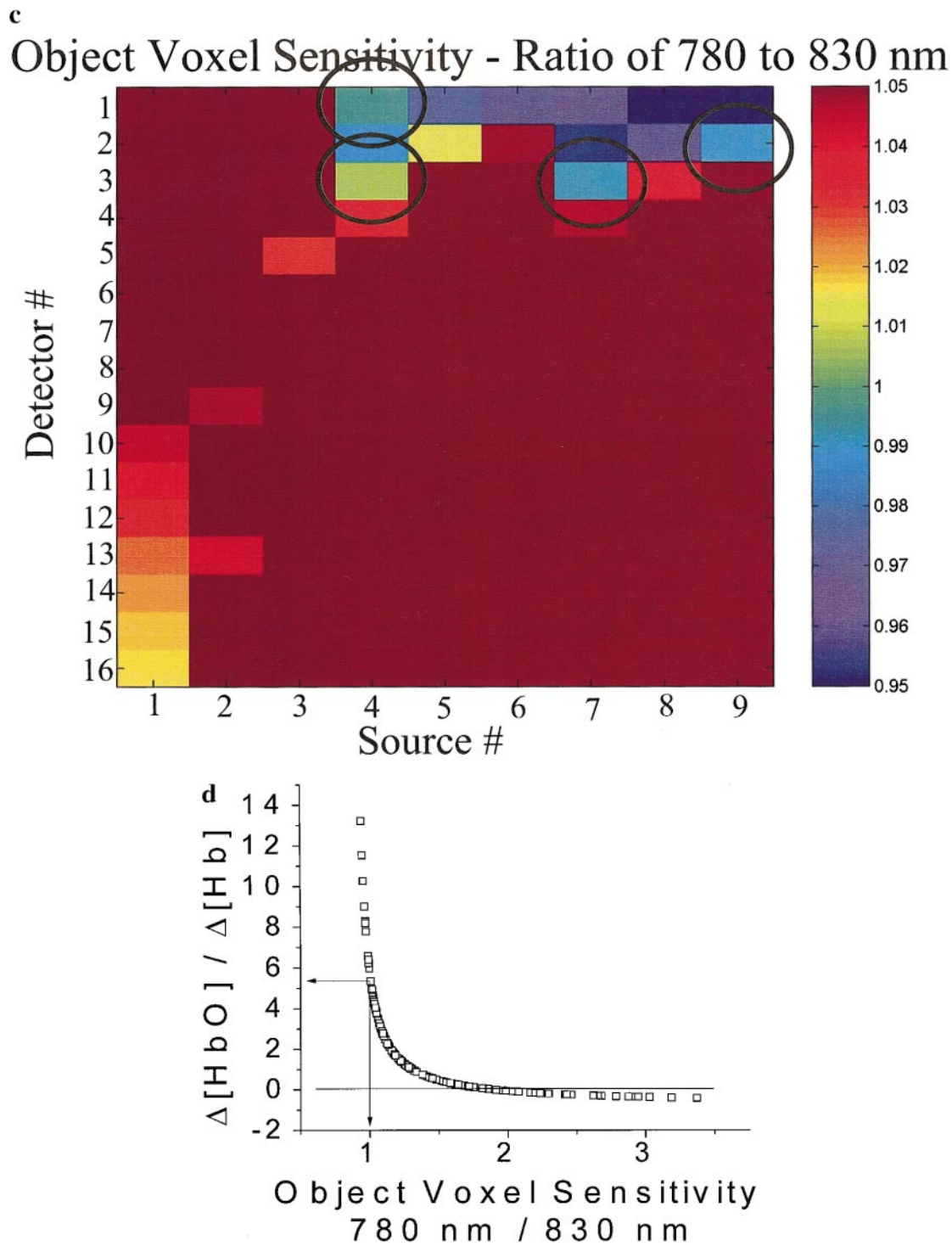


FIG. 6—Continued

FIG. 6. A review of the NIRS results obtained for each source-detector pair compared to the calculated sensitivity to the absorbing object. (a) The ratio of $\Delta[\text{HbO}]$ to $\Delta[\text{Hb}]$, which ranges from slightly less than 0 to 13. (b) The corresponding sensitivity that each measurement has to the absorbing object. The sensitivity is shown as a ratio of the sensitivity at 780 nm to that at 830 nm. (c) The color scale is windowed to more clearly indicate which source-detector pairs have a sensitivity ratio near 1. (d) A plot of the ratio of $\Delta[\text{HbO}]$ to $\Delta[\text{Hb}]$ versus the corresponding sensitivity ratio. Each point corresponds to one of the 144 measurements.

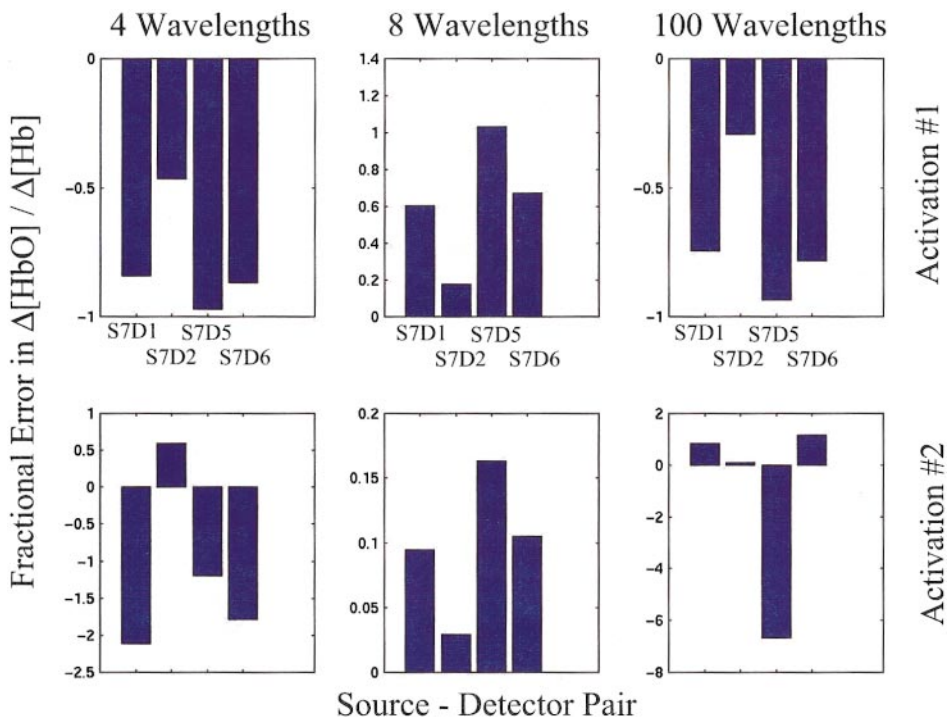


FIG. 7. The fractional error in the ratio $\Delta[\text{HbO}]/\Delta[\text{Hb}]$ for different numbers of wavelengths and different activations. Details are provided under Methods.

the analysis showed a wide variance in the ratio of $\Delta[\text{HbO}]$ to $\Delta[\text{Hb}]$ obtained from different source-detector pairs. This result could actually be correct and result from real underlying spatial variation in the concentration changes. However, our simulations of the human subject experiment indicate that under ideal conditions the standard MBLL analysis is unable to accurately determine the relative concentration changes.

Although the primary purpose of the neonate study was not to investigate the physiology of focal brain activation in the neonate, it is interesting to note that the optical results from this single study would be considered atypical in adult brain, since an increase in $[\text{Hb}]$ is counter to the change normally recorded using blood oxygen level dependent (BOLD) signal obtained using magnetic resonance imaging. However, similar results have been obtained in infants using MRI (33) and optical techniques (34). More DOT studies would be needed in order to confirm our result. A comprehensive NIRS study based on the MBLL analysis, on the other hand, would be unlikely to provide accurate information even with more subjects since the intrasubject results were so highly dependent upon source-detector geometry, an observation consistent with previous reports by others (35).

The wide variation seen in the MBLL analysis for the ratio of $\Delta[\text{HbO}]$ to $\Delta[\text{Hb}]$ results from differential sensitivity of the 780 and 830 nm measurement to the

focal change. As we see from Eq. (13), differential sensitivity results in cross-talk between oxy- and deoxy-hemoglobin. That is, a real change in oxyhemoglobin can look like a change in deoxyhemoglobin and vice versa. Our time-course data presented in Fig. 2 supports the cross-talk prediction as the initial increase in deoxyhemoglobin has the same characteristics as the increase in oxyhemoglobin. Equation (13) explicitly shows the cross-talk for a measurement with two wavelengths. A general equation can be derived to calculate the cross-talk for measurements with N wavelengths to prove that more wavelengths does not reduce the cross-talk error, as supported by our simulations.

There are a couple of approaches that can minimize the observed cross-talk. Measurements could be made at wavelengths for which the optical properties of the medium are nearly the same in which case the partial-volume effect will be constant for the different wavelengths. In this case, the determined concentration changes will be smaller than the real changes, but the relative values will be accurate. Another approach that can be applied to data collected at more than two wavelengths involves examining the residuals in the spectral analysis. The parameters of a model accounting for the spatial variation in the concentration changes can then be altered to minimize the residuals. This latter approach has promise and is left for future work.

SUMMARY

We have investigated the accuracy of using the Modified Beer-Lambert Law (MBLL) to analyze measurements of focal changes in the absorption coefficient of highly scattering media. The MBLL has long been used for analyzing the measurements of *global* changes in the absorption coefficient, but there has been no discussion of the systematic errors that arise when the analysis is applied to *focal* changes. This discussion is important now because of the increasing application of the MBLL for analyzing data from focal brain activation which necessarily causes a focal change in the absorption of hemoglobin within the cortex. Our results show that the MBLL analysis of focal changes (1) generally underestimates the hemoglobin concentration changes because of the partial volume effect and (2) because of the differential wavelength sensitivity, causes systematic errors in the concentration changes which depends on the position of the focal change relative to the source and detector positions. This last observation is significant because it means that a MBLL analysis can produce just about any result due to uncontrolled changes in source-detector positions and background optical properties of the medium. It is therefore prudent that researchers take extreme care when interpreting their standard NIRS analysis of focal changes caused by, for instance, brain activation. This observation has been made by Kleinschmidt *et al.* (35) from measurements in the adult human sensorimotor cortex during a unilateral finger opposition task. This problem will potentially be solved by diffuse optical tomography which uses a multiplicity of measurements in order to deconvolve the differential wavelength sensitivities to reconstruct images of the focal change. Finally, it may be possible to develop models that account for spatial variation when analyzing non-imaging NIRS data to reduce these systematic errors.

ACKNOWLEDGMENTS

The authors gratefully acknowledge Bruce Rosen and Sean Marrett for useful discussions leading to this paper and Susan Hintz and David Benaron for their enthusiasm for collecting the neonate data. D.A.B. acknowledges financial support from NIH 1 N29 NS38842 A 01 and from the Center for Minimally Invasive Therapies. This research was also funded in part by the U.S. Army, under Cooperative Agreement No. DAMD17-99-2-9001. This publication does not necessarily reflect the position or the policy of the Government, and no official endorsement should be inferred. G.S. acknowledges support from the NRSA under NIH-NINDS F32-NS10567.

REFERENCES

1. Neuman, M. R. 1987. Pulse oximetry: Physical principles technical realization and present limitations. *Adv. Exp. Med. Biol.* **220**: 135-144.
2. Severinghaus, J. W., and Honda, Y. 1987. History of blood gas analysis. VII. Pulse oximetry. *J. Clin. Monit.* **3**: 135-138.
3. Jobsis, F. F. 1977. Noninvasive infrared monitoring of cerebral and myocardial sufficiency and circulatory parameters. *Science* **198**: 1264-1267.
4. Cope, M., and Delpy, D. T. 1988. System for long-term measurement of cerebral blood flow and tissue oxygenation on newborn infants by infra-red transillumination. *Med. Biol. Eng. Comput.* **26**: 289-294.
5. Cope, M. 1991. *The Development of a Near-Infrared Spectroscopy System and Its Application for Noninvasive Monitoring of Cerebral Blood and Tissue Oxygenation in the Newborn Infant*. Univ. College London, London.
6. Kurth, C. D., Steven, J. M., *et al.* 1993. Near-infrared monitoring of cerebral circulation. *J. Clin. Monit.* **9**: 163-170.
7. Villringer, A., and Chance, B. 1997. Non-invasive optical spectroscopy and imaging of human brain function. *Trends Neurosci.* **20**: 435-442.
8. du Plessis, A. J. 1995. Near-infrared spectroscopy for the in-vivo study of cerebral hemodynamics and oxygenations. *Curr. Opin. Pediatr.* **7**: 632-639.
9. Nollert, G., Shinoka, T., *et al.* 1998. Near-infrared spectrophotometry of the brain in cardiovascular surgery. *Thorac. Cardiovasc. Surg.* **46**: 167-175.
10. Arridge, S. R. 1999. Optical Tomography in medical imaging. *Inverse Problems* **15**: R41-R93.
11. Dijkhuizen, R. M., Berkelbach van der Sprenkel, J. W., *et al.* 1997. Regional assessment of tissue oxygenation and the temporal evolution of hemodynamic parameters and water diffusion during acute focal ischemia in rat brain. *Brain Res.* **750**: 161-170.
12. Kwong, K. K., Belliveau, J. W., *et al.* 1992. Dynamic magnetic resonance imaging of human brain activity during primary sensory stimulation. *Proc. Natl. Acad. Sci. USA* **89**: 5675-5679.
13. Ogawa, S., Tank, D., *et al.* 1992. Intrinsic signal changes accompanying sensory stimulation: Functional brain mapping with magnetic resonance imaging. *Proc. Natl. Acad. Sci. USA* **89**: 5951-5955.
14. Mayhew, J., Zheng, Y., *et al.* 1999. Spectroscopic analysis of changes in remitted illumination: The response to increased neural activity in brain. *Neuroimage* **10**: 304-326.
15. Malonek, D., and Grinvald, A. 1996. Interactions between electrical activity and cortical microcirculation revealed by imaging spectroscopy: Implications for functional brain mapping. *Science* **272**: 551-554.
16. Pogue, B. W., Patterson, M. S., *et al.* 1995. Initial assessment of a simple system for frequency domain diffuse optical tomography. *Phys. Med. Biol.* **40**: 1709-1729.
17. O'Leary, M. A., Boas, D. A., *et al.* 1995. Experimental images of heterogeneous turbid media by frequency-domain diffusing-photon tomography. *Optics Letters* **20**: 426-428.
18. Delpy, D. T., Cope, M., *et al.* 1988. Estimation of optical path-length through tissue from direct time of flight measurement. *Phys. Med. Biol.* **33**: 1433-1442.
19. Wray, S., Cope, M., *et al.* 1988. Characteristics of the near infrared absorption spectra of cytochrome aa3 and hemoglobin for the noninvasive monitoring of cerebral oxygenation. *Biochim. Biophys. Acta* **933**: 184-192.
20. Matcher, S. J., Elwell, C. E., *et al.* 1995. Performance comparison of several published tissue near-infrared spectroscopy algorithms. *Analytical Biochemistry* **227**: 54-68.
21. Ishimaru, A. 1978. *Wave Propagation and Scattering in Random Media*. Academic Press, San Diego.
22. Patterson, M. S., Chance, B., *et al.* 1989. Time resolved reflectance

- tance and transmittance for the non-invasive measurement of tissue optical properties. *Applied Optics* **28**: 2331–2336.
23. Haskell, R. C., Svaasand, L. O., *et al.* 1994. Boundary conditions for the diffusion equation in radiative transfer. *J. Opt. Soc. of Am. A* **11**: 2727–2741.
 24. Furutsu, K., and Yamada, Y. 1994. Diffusion approximation for a dissipative random medium and the applications. *Phys. Rev. E* **50**: 3634.
 25. Durduran, T., Chance, B., *et al.* 1997. Does the photon diffusion coefficient depend on absorption? *J. Opt. Soc. Am. A* **14**: 3358–3365.
 26. Farrell, T. J., Patterson, M. S., *et al.* 1992. A diffusion theory model of spatially resolved, steady state diffuse reflectance for the noninvasive determination of tissue optical properties in vivo. *Medical Physics* **19**: 879–888.
 27. Jackson, J. D. 1975. *Classical Electrodynamics*. New York, John Wiley & Sons. 2nd.
 28. Kak, A. C., and Slaney, M. 1988. *Principles of Computerized Tomographic Imaging*. IEEE Press, New York.
 29. Arridge, S. R., and Hebden, J. C. 1997. Optical Imaging in Medicine: II. Modelling and reconstruction. *Phys. Med. Biol.* **42**: 841–854.
 30. Steinmetz, H., Furst, G., *et al.* 1989. Craniocerebral topography within the international 10-20 system. *Electroencephalogr. Clin. Neurophysiol.* **72**: 499–506.
 31. van der Zee, P., Cope, M., *et al.* 1992. Experimentally measured optical pathlengths for the adult's head, calf and forearm and the head of the newborn infant as a function of interoptode spacing. *Adv. Exp. Med. Biol.* **316**: 143–153.
 32. Heekeren, H. R., Kohl, M., *et al.* 1999. Noninvasive assessment of changes in cytochrome-c oxidase oxidation in human subjects during visual stimulation. *J. Cereb. Blood Flow Metab.* **19**: 592–603.
 33. Martin, E., Joeri, P., *et al.* 1999. Visual processing in infants and children studied using functional MRI. *Pediatr. Res.* **46**: 135–140.
 34. Meek, J. H., Firbank, M., *et al.* 1998. Regional hemodynamic responses to visual stimulation in awake infants. *Pediatr. Res.* **43**: 840–843.
 35. Kleinschmidt, A., Obrig, H., *et al.* 1996. Simultaneous recording of cerebral blood oxygenation changes during human brain activation by magnetic resonance imaging and near-infrared spectroscopy. *J. Cereb. Blood Flow Metab.* **16**: 817–826.
 36. Hintz, S. R., Benaron, D. A., Siegel, A. M., Stevenson, D. K., Boas, D. A. 1999. Real-time functional imaging of the premature infant brain during passive motor activation. *Pediatr. Res.* **45**: 2021.